HHS Public Access

Author manuscript

Neuron. Author manuscript; available in PMC 2022 February 17.

Published in final edited form as:

Neuron. 2021 February 17; 109(4): 690–699.e5. doi:10.1016/j.neuron.2020.11.023.

Midbrain activity shapes high-level visual properties in primate temporal cortex

Amarender R. Bogadhi[*,1,4,5], **Leor N. Katz**[*,1], **Anil Bollimunta**[1,6], **David A. Leopold**[2,3], **Richard J. Krauzlis**[1,†]

[1]Laboratory of Sensorimotor Research, National Eye Institute, National Institutes of Health, Bethesda, Maryland 20892 USA

[2]Laboratory of Neuropsychology, National Institute of Mental Health, National Institutes of Health, Bethesda, Maryland 20892 USA

[3]Neurophysiology Imaging Facility, National Institute of Mental Health, National Institute of Neurological Disorders and Stroke, National Eye Institute, National Institutes of Health, Bethesda, Maryland 20892 USA

[4]Hertie Institute for Clinical Brain Research, University of Tuebingen, Tuebingen 72076 Germany

[5]Werner Reichardt Centre for Integrative Neuroscience, University of Tuebingen, Tuebingen 72076 Germany

[6]Inscopix, Inc., Palo Alto, 94303 California USA

Summary

Recent fMRI experiments identified an attention-related region in the macaque temporal cortex, here termed fSTS, as the primary cortical target of superior colliculus (SC) activity. However, it remains unclear which aspects of attention are processed by fSTS neurons, and how or why these might depend on SC activity. Here we show that SC inactivation decreases attentional modulations in fSTS neurons by increasing their activity for ignored stimuli in addition to decreasing their activity for attended stimuli. Neurons in fSTS also exhibit event-related activity during attention tasks linked to detection performance, and this link is eliminated during SC inactivation. Finally, fSTS neurons respond selectively to particular visual objects, and this selectivity is markedly reduced during SC inactivation. These diverse, high-level properties of fSTS neurons all involve visual signals that carry behavioral relevance. Their dependence on SC activity could reflect a circuit that prioritizes the cortical processing of events detected subcortically.

Corresponding Authors: richard.krauzlis@nih.gov, bogadhi.amar@gmail.com, leor.katz@gmail.com.

*These authors contributed equally

†Lead Contact

Author Contributions

All authors designed the experiments. A.R.B., L.N.K., and A.B. conducted experiments and collected the data. A.R.B. and L.N.K analyzed the data. All authors interpreted the results. R.J.K., A.R.B. and L.N.K. wrote the manuscript.

Declaration of Interests: The authors declare no competing interests.

Graphical Abstract

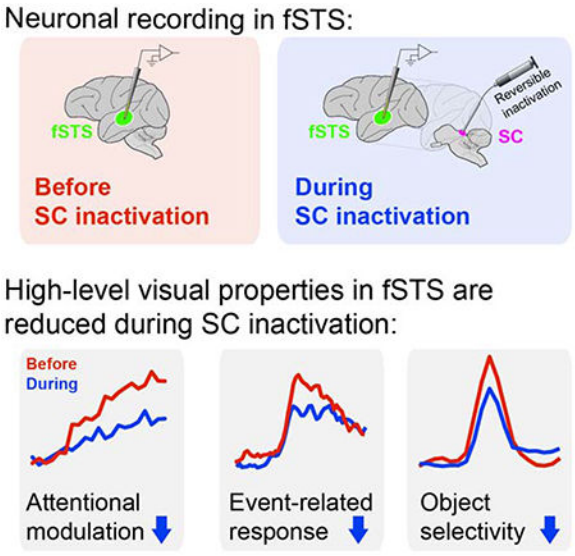

In brief

Bogadhi and Katz et al. determine how activity from the midbrain superior colliculus (SC) is necessary for the expression of high-level visual properties – attention-related modulation, event-detection activity and object-selective responses – in a newly identified region of the temporal cortex (fSTS) in primates.

Introduction

The superior colliculus (SC) in the dorsal midbrain is crucial for the control of visual selective attention and choice behaviors in many species (Krauzlis et al., 2018). In humans and other primates, where visual cortices play a conspicuous role in the expression of selective attention (Squire et al., 2013) and perceptual decisions (Gold and Shadlen, 2007), the contributions of the SC are a topic of ongoing debate (Basso and May, 2017; Krauzlis et al., 2013). Artificially manipulating SC activity causes large changes in perceptual task performance (Cavanaugh and Wurtz, 2004; Lovejoy and Krauzlis, 2010) but without altering neuronal processing in extra-striate visual areas (Zénon and Krauzlis, 2012), raising questions about where the SC exerts its effects (Sridharan et al., 2017). Despite the importance of the SC for selective attention and perceptual choices, the circuit linking the SC to cortical mechanisms has not yet been clearly identified.

We identified one possible link in a previous study in the macaque, in which we combined fMRI mapping with reversible inactivation of SC during a visual attention task and identified areas of cerebral cortex whose attentional modulation depended on activity in the SC (Bogadhi et al., 2019). The largest reduction in attention-related BOLD modulation following SC inactivation was observed in a circumscribed patch of cortex in the floor of the superior temporal sulcus, which we refer to as the fSTS (figure 1a–c; (Bogadhi et al., 2019). The location of this fSTS region corresponds roughly to the attention-related temporal cortex

regions described in several recent findings (Bogadhi et al., 2018; Caspari et al., 2015; Patel et al., 2015; Stemmann and Freiwald, 2019). Manipulating this cortical region directly using either reversible inactivation (Bogadhi et al., 2019) or local electrical microstimulation (Stemmann and Freiwald, 2019) significantly influenced attention-task performance, highlighting the direct role of this area in the control of covert attention. However, in order to understand how the fSTS region contributes to visual selective attention and why it depends on SC activity, it is necessary to identify the properties of neurons in fSTS, how these neuronal properties relate to behavior, and crucially, how they change following manipulations to SC.

Here we systematically investigate the responses of single neurons in fSTS in the context of a visual attention task and determine the response properties that are affected by inactivation of the superior colliculus. We demonstrate that neuronal responses in the fSTS are strongly modulated by the monkey's cued deployment of spatial attention, are highly sensitive to behaviorally relevant events, and closely follow the monkeys' detection behavior. Using a separate passive viewing task, we also demonstrate that fSTS neurons show selective responses to simple visual objects. Most importantly, each of these higher-order visual properties – attention-related modulation, event detection, and object selectivity – were strongly compromised at the single neuron level during inactivation of the SC in the midbrain. The results demonstrate an important and causal contribution of SC activity to high-level visual operations in a newly described region of the primate ventral stream, at the convergence of selective attention and object selectivity. We suggest that the SC provides a relatively coarse signal that prioritizes the cortical processing of feature properties for behaviorally relevant events.

Results

Monkeys were trained to perform a covert attention task in which they reported relevant stimulus changes by releasing a joystick while maintaining central fixation for the entirety of the trial. In the *Attend* condition (figure 1a), monkeys reported an abrupt change in the direction of motion applied to either of two peripheral visual stimuli. In the *Ignore* condition (figure 1b), monkeys were required to ignore these direction changes in the peripheral stimuli and instead report a dimming of the central fixation spot. The magnitude of direction change was adjusted to keep the task demanding and the detection performance at near threshold – animals correctly responded in 73% ± 14% of trials in the *Attend* condition and 62% ± 13% in the *Ignore* condition (mean ± sd of both monkeys, see figure 1a, b for individual performance).

Neuronal recordings were targeted based on the functional identification of the fSTS region, using a combination of fMRI mapping and SC inactivation during a block-design version of the attention task (figure 1c) (see (Bogadhi et al., 2019)). From chambers placed over the fSTS region in both monkeys, we recorded the activity of 972 single neurons during interleaved *Attend* and *Ignore* blocks of trials. These data were collected over a total of 24 sessions, including 16 sessions in which the intermediate layers of the SC were reversibly inactivated (see Methods). We first investigated the spatial distribution of fSTS neurons showing attentional modulation in the absence of SC inactivation. Attentional modulation

was computed as the area under the curve (AUC) for spike counts in the *Attend* vs. *Ignore* conditions (see Methods). Sampling neurons across chamber positions, we found a "hotspot" of attention-related modulation in a restricted region of the STS floor spanning a volume of approximately $12mm^3$, consistent with the fMRI-defined fSTS region (figure 1d). Overall, these fSTS neurons displayed strong attention-related modulation in the population average (figure 2a) and in individual cells (figure 2c, top; Wilcoxon signed-rank test, $p < 2e\text{-}47$), which gradually evolved over time starting from stimulus onset (supplementary figure 1b). These results demonstrate a strong attention-related modulation in the fSTS neurons, regardless of the measure used (see supplementary figure 1 for a comparison of AUC and AMI).

SC contributes to attention-related modulation in fSTS neurons

We next investigated how the attention-related modulation of single neurons was affected by reversible inactivation of the SC. We confirmed that microinjection of muscimol into the SC caused major deficits in both saccade and attention task performance; consistent with previous findings (Lovejoy and Krauzlis, 2010), the deficits were spatially restricted to portions of the visual field contralateral to the injection site (supplementary figure 2).

The attentional modulation of fSTS neurons was markedly reduced by SC inactivation, as was evident in the population averages of discharge rate over time (figure 2a, b), as well as in the attention-related modulation (AUC) of individual neurons in our population (figure 2c; Wilcoxon rank-sum test, $p < 3e\text{-}12$). This dampening of attentional modulation could be observed as early as stimulus onset when the attentional modulation started to emerge in the fSTS population (supplementary figure 1), showing that the effect of SC inactivation is a scaling down rather than a delay of attentional modulation in fSTS neurons. Using a traditional attention modulation index (AMI) instead of AUC, SC inactivation reduced the median AMI by 45.9%, from 0.11 to 0.06 (supplementary figure 1). This is an especially large drop considering that we included all neurons in our population and did not sub-select neurons based on responsiveness or attentional modulation amplitude, thereby minimizing any bias of inclusion criterion in our findings. These reductions in fSTS attention-related modulation stand in contrast to previous findings in other portions of extrastriate visual cortex, where SC inactivation led to no or minimal reduction in observed attentional modulation (Zénon and Krauzlis, 2012). Crucially, the reduction in modulation was present across sessions of SC inactivation (figure 2d; Wilcoxon signed-rank test, $p < 0.002$), and was not evident during control injections of saline (supplementary figure 3).

We quantified the consequences of SC inactivation on fSTS activity using the AUC (or AMI) because such measures are not affected by general scaling of activity due to, say, changes in arousal. Instead, these measures are influenced by the differential scaling between conditions. Indeed, the population averages (figures 2a, b) showed a differential pattern in which *Attend* activity was reduced but *Ignore* activity was increased. Neither the decrease in *Attend* activity nor the increase in *Ignore* activity were statistically significant on their own (supplementary figure 4a). Only when considered jointly were the effects of SC inactivation on fSTS activity significant. These observations show that the effect of SC

inactivation on fSTS activity is a selective reduction of attentional modulation and not due to an overall scaling of activity.

The substantial reductions in attentional modulation cannot be explained by overall changes in population firing rates during the delay period or other epochs of the attention task, response latencies or tuning properties, since these were unaffected by SC inactivation (supplementary figure 4). Also, reductions in attention-related modulation cannot be attributed to microsaccades because the reductions were observed even in trials without microsaccades (supplementary figure 5). Together, these findings demonstrate that the dependence of fSTS attentional modulation on SC activity is not an indirect effect or due to non-specific inputs to fSTS. Rather, it is directly attributable to the role of the SC in supporting attentional selectivity in fSTS.

SC contributes to change-evoked activity in fSTS neurons

In addition to strongly reflecting the monkey's internal attentional state, neurons in fSTS also responded vigorously to task-relevant stimulus events in the contralateral field (figure 3a). In this case, the events were subtle but abrupt directional changes that the monkey had been trained to detect in order to receive a reward. Importantly, inactivation of the SC significantly attenuated this change-evoked activity (figure 3b), similar to the reduction in cued attention-related modulation described above. This decrease was observed in the population of single neurons (figure 3c; Wilcoxon rank-sum test, $p < 4e\text{-}3$), and across sessions (figure 3d; Wilcoxon signed-rank test, $p < 0.03$). Additionally, the magnitude of the change-evoked response, quantified as the mean increase in firing rate following the change (0.2 to 0.5 s time window) relative to pre-change firing rate (−0.5 to 0 s), was reduced during SC inactivation in both the *Attend* and the *Ignore* conditions (Wilcoxon rank sum test. $p < 4e\text{-}23$ and $p < 3e\text{-}18$, respectively). These findings show that fSTS neurons signal stimulus changes relevant to the behavior, and most importantly, that these change-evoked neuronal signals depend on midbrain activity.

SC contributes to detection-related modulation in fSTS neurons

We next tested whether the trial-by-trial variation in fSTS neural responses to contralateral stimulus changes during the *Attend* condition were correlated with the monkey's detection behavior. In the absence of SC inactivation, we found that change-related spiking responses were consistently stronger to detected changes ("hits") than to undetected changes ("misses") (figure 4a). However, SC inactivation strongly affected the correlation of fSTS neurons to behavioral performance, specifically resulting in a much-reduced difference in the spikes elicited during "hits" and "misses" (figure 4b). We used a *detect probability* measure (Cook and Maunsell, 2002) to evaluate and quantify this trial-by-trial relationship and its dependence on SC activity (see Methods). Before SC inactivation, detect probabilities were significantly greater than chance (figure 4c, top; Wilcoxon signed-rank test, $p < 3e\text{-}12$). However, during SC inactivation, detect probabilities were substantially reduced for both the population of individual neurons (figure 4c; Wilcoxon rank-sum test, $p < 3e\text{-}4$) and across sessions (figure 4d; Wilcoxon signed-rank test, $p < 0.03$). Control saline injections again confirmed that these effects required suppression of SC activity (supplementary figure 3). These reductions in detect probability show that the degree to

which fSTS activity predicted animal's detection behavior on a trial-by-trial basis also depends on SC activity.

SC contribution to attention-related properties in fSTS is not specific to visual motion

We investigated if the attention-related properties in fSTS neurons and their loss during SC inactivation were specific to the motion stimulus used. We trained monkey #1 on a version of the attention task where we replaced the motion with dynamic white noise and the motion direction-change event with a 0.5 s second-order orientation pulse (figure 5a; see Methods). Importantly, we confirmed that the brief orientation pulse cannot be detected based on motion (Bogadhi et al., 2019), and the monkeys' detection performance was at threshold (figure 5b). We also confirmed that SC inactivation significantly reduced the detection ("hit rate") of brief pulses contralateral to the inactivated SC (supplementary figure 2c), consistent with performance deficits in the motion task.

Neuronal recordings in the second-order orientation task revealed attention-related modulations among fSTS neurons (figure 5c, e), similar to the motion stimulus (figure 2) and consistent with the previous fMRI results (Bogadhi et al., 2018). Crucially, SC inactivation reduced each of the neuronal measures reported in fSTS neurons–attention-related modulation (figure 5c–e), change-evoked activity (figure 5f–h), and detect probabilities (figure 5i–k). These findings demonstrate that the SC's contribution to attentional modulation and event detection properties of fSTS neurons is not contingent on a particular stimulus or visual feature such as motion, consistent with both the SC and fSTS playing major roles in the control of spatial attention regardless of the specific visual feature (Bogadhi et al., 2019; Krauzlis et al., 2013).

SC contributes to object selectivity in fSTS neurons

How might the SC activity exert its influence on fSTS? One possibility involves the relay of visual information through the thalamic pulvinar, which receives strong input from the SC (Harting et al., 1980) and projects to areas in the STS (Boussaoud et al., 1992; Dominguez-Vargas et al., 2017). Based on the strong colliculo-pulvinar input to the STS and the well-known selectivity for visual objects exhibited by STS neurons in related regions (Hung et al., 2005; Rolls, 2000; Tsao et al., 2003), we suspected that fSTS neurons would exhibit object selectivity. We asked whether this selectivity, if present, might also depend on activity through pathways linking the SC to fSTS.

We trained monkeys to passively view a stream of briefly (0.25 s) flashed images of visual objects within the receptive fields of neurons recorded in fSTS. To control for low-level visual features, we also included grid- and phase-scrambled versions of the same images randomly intermixed in the stream (figure 6a). Neurons in fSTS exhibited strong selectivity among the particular visual objects in our stimulus set. For example, some neurons responded vigorously to the presentation of specific images (e.g., "water bottle"), but not to any of the other intact or scrambled images (figure 6b). Across the population of 303 neurons, 92 showed significant selectivity for at least one object (figure 6c). This neural selectivity could not be attributed to attention drawn to particular images, since simultaneously recorded neurons exhibited selectivity for different images (e.g., units #54,

#57 & #58 in figure 6b). The rapid rise, strength, response transience, and overall prevalence of object selectivity was evident in the population responses (figure 6d) and in the distribution of object selectivity values (figure 6f top; median = 0.56, significantly greater than 0.5, Wilcoxon signed-rank test, $p < 6e\text{-}49$).

During SC inactivation, the number of object-selective neurons was substantially reduced from 30.3% (92/303) to 17.89% (51/285) (figure 6c; Chi-square test, $p < 7e\text{-}4$). Significant reductions in object-selectivity during SC inactivation were evident in both population responses (figure 6d, e) and in our sample of individual neurons (figure 6f; Wilcoxon rank-sum test, $p < 4e\text{-}4$). The reduction in object-selectivity was consistent across sessions (Figure 6g; Wilcoxon signed-rank test, $p < 0.04$) and was likely due to a reduction in the phasic responsiveness of fSTS neurons to images in this task when SC activity was suppressed (supplementary figure 6). This finding demonstrates that fSTS neurons gain their basic visual object selectivity and responsivity, in part, through a pathway that involves the SC.

Effects of SC inactivation on continuously isolated fSTS neurons

Finally, we determined whether the four main effects of SC inactivation on fSTS neurons – reductions in attention-related modulation, change-evoked activity, detect probability and object selectivity – were also evident on the level of single neurons, in addition to the population-level observations (figures 2, 3, 4 and 6). We adopted a method for tracking individual neurons across the “before” and “during” phases of SC inactivation experiments to identify a subpopulation of fSTS neurons that are most likely to be identical in both the “before” and “during” phases (see methods; (Herman et al., 2020)). This approach reduced our statistical power (255 of 380 neurons recorded “before” were identified as “continuously isolated”) but enabled us to evaluate the effect of SC inactivation at the level of single neurons. We found that the subpopulation of continuously isolated fSTS neurons was significantly affected by SC inactivation (figure 7), and exhibited reductions in attention-related modulation ($p < 3e\text{-}9$, Wilcoxon signed-rank test), change-evoked activity ($p < 0.02$), detect probability ($p < 2e\text{-}3$), and object selectivity ($p < 2e\text{-}12$). For each of these four measures, we also quantified the proportions of fSTS neurons that lost or gained significant modulation following SC inactivation (figure 7, insets). A comparison of these proportions further shows that SC inactivation has a deteriorating influence on all four visual properties of fSTS neurons – attention-related modulation ($p < 2e\text{-}4$, Chi-square proportion test), change-evoked activity ($p = 0.081$), detect probability ($p = 0.085$) and object selectivity ($p < 7e7$). Thus, regardless of whether we took a population approach, by treating “before” and “during” as two independent datasets (figures 2, 3, 4 and 6), or a single neuron approach, by constructing a subpopulation of continuously isolated neurons in both “before” and “during’ datasets (figure 7), our main findings that SC causally contributes to high-level visual properties in fSTS neurons remained consistent.

Discussion

Our results show that neurons in fSTS exhibit a number of properties linked to high-level visual operations in the primate brain, and crucially, that these properties are dependent on

midbrain SC activity. First, neurons in fSTS exhibited a large attention-related modulation during the delay period of the selective attention task (figure 2a); this modulation did not depend on the specific visual feature used in the attention task (figure 5c). Second, fSTS neurons showed a vigorous response to contralateral stimulus changes (figure 3a). Third, the size of this change-evoked activity was correlated with monkey's detection performance in the task (figure 4a). Fourth, fSTS neurons exhibited object selectivity with strong responses to particular visual objects (figure 6c). Most importantly, all four of these neuronal response properties were significantly reduced during inactivation of the SC, both at the population-level (figures 2, 3, 4 and 6) and for the subpopulation of "continuously isolated" neurons (figure 7). For the attention modulation in particular, SC inactivation decreased the activity for attended stimuli but increased the activity for ignored stimuli, resulting in a significant loss of attention selectivity for fSTS neurons. Overall, these results demonstrate an important causal contribution of the midbrain SC activity to high-level visual operations in a region of the primate temporal cortex where selective attention, event detection and object selectivity converge.

Our results identify neurons within the fSTS region as participating in a circuit for selective attention control that depends on SC activity. The properties of this SC-dependent control mechanism are different from the well-known mechanisms centered in the prefrontal cortex, which are thought to provide feedback signals to early visual areas for regulating how basic visual features are processed (Squire et al 2013). First, fSTS lies at a later stage in the hierarchy of cortical areas processing basic visual features (Felleman and Van Essen, 1991; Hilgetag et al., 2000). Second, the control of the fSTS region by the SC is not specific to a particular visual feature (figure 5). Indeed, the properties of fSTS neurons affected by SC inactivation in our experiments form a seemingly curious collection – selective responses to motion, to second-order orientation, and to flashed objects. We speculate that this intriguing set of properties might be defined by their behavioral relevance to the subject. Third, the changes in fSTS caused by SC inactivation omitted two signatures of selective attention typically found in earlier visual areas – neither spike-count correlations nor Fano factor (Cohen and Newsome, 2009; Mitchell et al., 2009) showed consistent effects during the attention deficits caused by reversible inactivation (supplementary figure 7). Importantly, while the SC and prefrontal control mechanisms have different properties, they are unlikely to operate independently. Indeed, inactivation of prefrontal regions also influence activity in fSTS, but to a lesser extent (Bogadhi et al., 2019). Teasing apart the distinct functional contributions of these different circuits is one the reasons we think that the current approach – electrophysiological recordings combined with causal manipulations, guided by fMRI results – is especially useful for understanding the neural mechanisms of selective attention in the primate brain.

These results provide at least a partial explanation for how suppression of SC activity can cause deficits in visual attention without affecting attention-related modulation in extrastriate cortex (Zénon and Krauzlis, 2012). Because loss of SC activity impacts attention at a later stage of hierarchical processing (Felleman and Van Essen, 1991), SC inactivation can cause large behavioral deficits in attention tasks without changing neuronal signatures of attention in earlier visual areas. The nested structure indicated by these results – a cascade of

feature-specific and feature-nonspecific sites of modulation – would be an efficient way to organize feedback about priors during attention-demanding visual tasks (Bondy et al., 2018).

The STS has recently been identified by multiple labs, including our own, as a novel node in the cortical control of attention (Bogadhi et al., 2018, 2019; Caspari et al., 2015; Patel et al., 2015; Stemmann and Freiwald, 2019). The anatomical overlap between fSTS and a recently identified attention-related region (PITd) in the STS (Stemmann and Freiwald, 2019) is yet unclear, but there is a functional resemblance: both fSTS and PITd exhibit attention-related modulations that are not specific for visual features and both exert causal influences on behavior in attention tasks (Bogadhi et al., 2019; Stemmann and Freiwald, 2019). A crucial distinction, however, is that the fSTS region targeted here was identified not by attention-related modulation alone, but by its causal dependence on SC.

Relatively little is known about this cortical fSTS region (Desimone and Ungerleider, 1986; Kilintari et al., 2014; Mysore et al., 2010; Rosenberg et al., 2008; Ward et al., 2015). Anatomically, fSTS lies posterior to previously described polysensory (Bruce et al., 1981) or biological motion areas (Jellema and Perrett, 2003) and anterior to motion sensitive areas such as MT and MST. It is unlikely that fSTS region overlaps with one of the known face or object patches because neurons in these patches are category selective (Tsao et al., 2006), and to the contrary, we observed neurons with selectivities for different categories, even when simultaneously recorded on nearby electrode sites (figure 6b). Additionally, we observed object selectivity in the early phasic part of the neural response, unlike neurons in the face and object patches which exhibit selectivity much later (Kreiman et al., 2006; Tsao et al., 2006). The phasic responses observed for both visual form in the object viewing task (figure 6d) and stimulus change in the attention task (figure 3a), regardless of stimulus feature (figure 5f), may be part of a general neural mechanism for tagging relevant objects and events in a visual scene.

The specific targeting of fSTS by activity from the SC is arguably its most distinctive feature, and we suspect that SC activity influences fSTS through a pathway involving the thalamic pulvinar (Boussaoud et al., 1992; Dominguez-Vargas et al., 2017; Harting et al., 1980). Similar ascending circuits from SC through higher-order thalamus to later stages of visual cortex have also been recently described in mice (Beltramo and Scanziani, 2019; Bennett et al., 2019; Tohmi et al., 2014). The functions of these SC-dependent circuits may complement those of the well-known geniculostriate visual pathways (Felleman and Van Essen, 1991; Hilgetag et al., 2000). We suggest that the SC may provide a relatively coarse signal about the occurrence of potentially task-relevant events. Sharing this signal with temporal cortical areas in the ventral stream could prioritize the processing of feature properties for that event, such that its identity and relevant meaning can be more fully and accurately estimated. Thus, the cortical visual system of primates might use signals from the SC as a “shortcut” for rapid object processing: before engaging feedforward hierarchical circuits to identify all possible objects in a scene, inputs from the SC might guide the rapid recognition of objects deemed most important at that moment.

STAR Methods

RESOURCE AVAILABILITY

Lead Contact—Further information and requests for resources and reagents should be directed to and will be fulfilled by the Lead Contact, Rich Krauzlis (richard.krauzlis@nih.gov).

Materials Availability—This study did not generate new unique reagents.

Data and Code Availability—The datasets and code supporting the current study have not been deposited in a public repository because we are analyzing other aspects of the datasets but are available from the corresponding authors upon request.

EXPERIMENTAL MODEL AND SUBJECT DETAILS

Animals—Two adult male rhesus monkeys (*Macaca mulatta*) weighing 7-9 kg were used in the study. All procedures and animal care were approved by the National Eye Institute Animal Care and Use Committee and complied with the Public Health Service Policy on the humane care and use of laboratory animals. We surgically implanted plastic head-posts and electrophysiology chambers, under isoflurane and aseptic conditions, to access the SC and the floor of the STS (fSTS). The placement of the fSTS chamber was guided by previously obtained functional imaging results (Bogadhi et al., 2019), and we targeted the fSTS region in different hemispheres across the two monkeys. Both monkeys were trained on an attention task (figure 1a, b), a visually guided saccade task (for mapping the affected region during SC inactivation, supplementary figure 2a), an object tuning task (figure 6a), and several other passive fixation tasks (for mapping spatial receptive fields and direction tuning of single neurons).

METHOD DETAILS

Experimental apparatus—Animals were seated and head-fixed in a primate chair (Crist Instrument Inc., Hagerstown, MD, and custom-built) inside a darkened booth at a distance of 48 cm from a VIEWPixx display (VPixx Technologies, Saint-Bruno, QC Canada) with a 1920 x 1200 resolution (~ 60° x 38°) and 100Hz frame-rate. Stimuli were presented on the VIEWPixx display that was controlled by a mid-2010 Mac Pro (Apple Inc., Cupertino, CA) running MATLAB (The Mathworks, Natick, MA) with the Psychophysics Toolbox extensions (Brainard, 1997). The background luminance of the screen across all tasks was 14 cd/m^2. Eye position was recorded using an EyeLink 1000 infrared eye-tracking system (SR Research Ltd., Ottowa, Ontario, Canada); this signal was monitored online to ensure strict fixation within a 2° fixation window during all tasks. The primate chairs were equipped with a single axis joystick (CH Products, model HFX-10) that the monkeys used to report relevant stimulus changes during the attention task. Joystick presses and releases were detected by a change in voltage signal. All experiments were controlled using a modified version of PLDAPS (Eastman and Huk, 2012).

Electrophysiology recording—Neuronal and behavioral signals (e.g. eye position, joystick) were acquired by an Omniplex system (Plexon Inc., Dallas, Texas). Neuronal

signals were recorded using a 24-channel linear array (V-probes, Plexon Inc., Dallas, Texas) that was introduced into the fSTS region by a custom built motorized micro-drive. Figure 1d shows coronal sections of fSTS region overlaid with colored spots representing average attention-related modulation (see below) of all neurons recorded in that grid hole. AP and ML location of the colored spots were determined by the grid hole; depth was determined as the average depths across recording sessions in that grid hole.

Entry into the target fSTS region was confirmed based on depth measurements compared to the MRI slices (figure 1d), and changes in neural activity observed during transitions from gray matter in the dorsal bank of the STS to sulcus, and from sulcus to gray matter in the target region of the fSTS. Upon entry into the target region we allowed the V-probe to settle and the neuronal activity to stabilize (~1 hour) before beginning the experimental session.

Each session began with an online mapping of spatial receptive fields to optimize stimulus placement for the subsequent tuning and attention tasks. Following the mapping, we collected neuronal responses during the direction tuning, attention, and object tuning tasks. At the end of the “before SC inactivation” set of tasks, we reversibly inactivated SC, and continued collecting data for the “during SC inactivation” set of tasks, starting with the attention task, followed by the tuning and receptive field mapping tasks. Overall, we performed 24 experimental sessions with the motion-change detection stimulus: 16 with muscimol injections into SC (9 in monkey #1; 7 in monkey #2), and 8 control sessions of saline injection and sham manipulation (monkey #1). Unless otherwise noted, results for the two monkeys were combined after confirming they were statistically significant in each individual animal (data not shown). Additionally, 6 experimental sessions with the orientation pulse detection stimulus were performed (monkey #1), all with muscimol injections into SC.

Receptive field mapping task—Spatial receptive fields of fSTS neurons were mapped in each experimental session before and during SC inactivation, while monkeys performed a passive fixation task. Monkeys started each trial by fixating a central square spot (0.21° wide; green color). Following 0.5 s of fixation, a random dot motion stimulus was presented briefly (0.25 s on and 0.25 s off) within a circular aperture (3° radius) at 100% coherence. The stimulus was presented at locations drawn randomly from an XY grid (5° spacing, covering the display) and at locations selected by the experimenter based on the neuronal responses. The direction of the motion stimulus was pseudo-randomized across stimulus presentations. Each trial lasted for 4 seconds and consisted of 6 stimulus presentations. Monkeys were required to maintain fixation within a 2° window for the full duration of the trial to receive a reward. We collected an average of 552 (before) and 522 (during) presentations in each experimental session.

After receptive field mapping, a location was selected by the experimenter which maximized the spatial overlap of receptive fields across the recording channels. This selected location was thereafter fixed for all subsequent tasks: the direction tuning task, the object tuning task, and the attention task, before and during SC inactivation. Overall, locations used ranged between 8 – 14° eccentricity across all sessions.

Direction tuning task—Direction tuning properties of fSTS neurons were mapped in each experimental session before and during SC inactivation, while animals performed a passive fixation task. The fixation task was similar to the receptive field mapping task, except that each brief motion stimulus presentation (0.25 s on and 0.25 s off) was presented at the fixed visual field location. Random dot motion was presented at 100% coherence and the direction of motion was selected pseudo-randomly on each stimulus presentation from one of the 12 directions (equally spaced from 0 to 360 degrees). A 0% coherence stimulus was also included. Each trial lasted for 4 seconds and consisted of 6 stimulus presentations. Overall, we collected an average of 40 (before) and 36 (during) presentations per motion direction in each experimental session.

Object tuning task—Monkeys performed a passive fixation task similar to the direction tuning task, except that the motion stimulus was replaced with static images containing objects (visual forms) and their corresponding grid- and Fourier phase-scrambled versions (figure 6a). A total of 21 unique images were used (7 object, 7 grid-scrambled and 7 phase-scrambled images) and all object images were corrected for luminance histogram and Fourier spectra using SHINE toolbox (Willenbockel et al., 2010), before generating their corresponding scrambled versions. Each image was presented briefly (0.25 s on and 0.25 s off) at the fixed location selected previously. Each trial lasted 4 seconds and consisted of 6 image presentations. Overall, we collected an average of 49 (before) and 40 (during) presentations per image in each experimental session.

Attention task—The attention task consisted of two main conditions: *Attend* and *Ignore* (figure 1a, b), plus two control conditions, *Attend Single Patch* and *Baseline*. In all task conditions, monkeys initiated the trial by pressing the joystick down and fixating a central square spot (50 cd/m^2). Following 0.3 s of fixation, a cue in the form of a colored square outline was flashed around the central fixation spot for 0.2 s. The width of the fixation spot was 0.21° and the width of the cue was 0.35°. The color of the cue instructed the monkeys to attend or ignore the peripheral motion stimuli and detect the relevant events. In the *Attend* and *Attend Single Patch* trials, the color of the central cue was red, indicating that the relevant event was a direction-change in the peripheral motion stimulus (detailed below). In the *Ignore* and *Baseline* trials, the color of the central cue was black, indicating that direction-change in the peripheral stimulus was irrelevant and the luminance change in the fixation spot was relevant. In all conditions, monkeys were required to maintain central fixation within a 2° fixation window for the full duration of the trial. All four task conditions were presented in a block design where each condition was presented once (in pseudo-random order) before advancing to the next block. Each block consisted of 150 trials: 54 *Attend*; 54 *Ignore*; 30 *Attend Single Patch*; and 12 *Baseline*. Monkeys completed an average of 5 blocks before SC inactivation and 4 blocks during inactivation across 16 sessions. The sequences of events in each condition are presented below.

In *Attend* trials, following 0.5 s after cue offset, two random-dot motion stimuli appeared on either side of the fixation spot in the contralateral and ipsilateral hemifields, symmetric to the vertical meridian. The location of the contralateral stimulus matched the location from mapping tasks (see Receptive field mapping section). Overall, location eccentricity ranged

between 8 – 14° across sessions. On 77.7% of *Attend* trials, one of the motion stimuli changed direction during 1-3.5 s after stimulus onset (uniform probability), and the monkeys responded by releasing the joystick within 0.3 – 0.8 s to receive a reward. On the remaining 22.3% trials, there was no stimulus change and monkeys were rewarded for maintaining fixation and continuing to hold the joystick pressed ("catch trials").

In *Ignore* trials, the peripheral motion stimuli and task sequence were identical to those in the *Attend* trials, but the monkeys were rewarded for ignoring the peripheral stimuli, and instead, responded to a change in fixation spot luminance (decrease of 1-2 cd/m^2 across sessions). On 77.7% of *Ignore* trials, the fixation spot luminance change occurred during 1–3.5 s after stimulus onset (uniform probability) and monkeys responded by releasing the joystick within 0.3 – 0.6 s to receive a reward. On the remaining 22.3% of trials, the fixation spot luminance remained unchanged, and monkeys were rewarded for maintaining fixation and continuing to hold the joystick pressed ("catch trials"). Independent of the luminance change, on 66.6% of the trials, one of the two motion stimuli changed direction and the monkeys were rewarded for ignoring the motion direction-change and responding to the change in the fixation spot luminance.

Attend Single Patch trials were identical to *Attend* trials, with only one of the two motion stimuli presented on any given trial. The stimulus was presented either at the same contralateral or ipsilateral location on equal number of trials.

Baseline trials were identical to *Ignore* trials, except that no peripheral stimulus was presented. In this condition, monkeys were simply required to detect a change in fixation spot luminance.

Random dot motion stimulus—Each random dot motion stimulus consisted of moving dots presented in a circular 3° radius aperture. The motion direction of each dot was drawn from a normal distribution with a mean value of 30° above horizontal (in all but one session) and a standard deviation of 16°, to be consistent with the previously performed fMRI study (Bogadhi et al., 2019). The lifetime (10 frames, 100 ms), density (25 dots/^{o2}/s), and speed of the dots (15 °/s) were held constant. Luminance of each moving dot in the motion patches was 50 cd/m^2. The change in direction of motion (Δ) ranged from 0.75 to 1.25 standard deviations of motion direction across monkeys and sessions.

Modified attention task: Orientation-pulse detection—In separate sessions, monkey #1 performed a modified version of attention task with the same conditions (*Attend, Ignore, Attend Single Patch, Baseline*), where random dot motion stimulus was replaced with dynamic white noise stimulus and motion-change event was replaced with a brief (0.5 s) second-order orientation pulse. In the *Attend* and *Attend Single Patch* conditions, the monkey reported the orientation pulse event by releasing the joystick within 0.3 - 0.8 s to get a reward, whereas in the *Ignore* condition, monkey ignored the orientation pulse event and reported the luminance decrease in the fixation spot by releasing the joystick within 0.3 - 0.6 s to get a reward. We collected an average of 6 blocks before SC inactivation and 5 blocks during SC inactivation across 6 sessions.

The white noise stimulus had a diameter of 6° and consisted of checks, each the size of a pixel, dynamically changing luminance on every frame at random, with luminance values ranging from 8 to 84 cd/m^2. The second-order orientation stimulus was generated by briefly (0.5 s) modulating the contrast of a white noise stimulus with a 2-dimensional sinusoid, whose spatial frequency and orientation was 0.7 cycles/deg and 90° respectively. Importantly, the mean luminance of the stimulus (38 cd/m^2) was held constant throughout its presentation and was constant across every band in the oriented grating. We refer to this as a second-order orientation stimulus, because the visibility of the oriented grating was due to local differences in contrast, not luminance, and we confirmed that the orientation pulse contained no change in motion energy (Bogadhi et al., 2019).

Reversible inactivation—Reversible inactivation of the intermediate layers of the SC (n = 22; monkey #1 (left hemisphere): 15, monkey #2 (right hemisphere): 7) was done by injecting muscimol (0.3-0.5 μl; 5 mg/ml) based on methods described previously (Lovejoy and Krauzlis, 2010). All candidate sites were first identified by neuronal recordings and electrical stimulation prior to the muscimol inactivation experiment. Injections were done using a custom-made apparatus (Chen et al., 2001) using an injection pump (Legato, KD Scientific) at a constant rate of 0.05 μl/min. For saline controls, the same volumes were injected at the same locations in the intermediate layers of the SC at the same rates.

Mapping of the impaired visual field—Thirty minutes after the end of the muscimol injection, we used a visually guided saccade task to map the affected visual field using methods described previously (Lovejoy and Krauzlis, 2010). We measured the peak velocity for saccades made to targets at different visual field locations before and during inactivation. The locations at which saccade peak velocities were reduced indicated the locus and the extent of the affected visual field (supplementary figure 2a).

QUANTIFICATION AND STATISTICAL ANALYSIS

Electrophysiology analysis—Electrophysiological data obtained from the linear arrays were sorted offline into single neurons using the *kilosort* algorithm followed by a manual curation in the *phy* software (Pachitariu et al., 2016). For analyses related to attention tasks, we included single neurons with an average trial firing rate greater than 1 spike/s in both *Attend* and *Ignore* blocks. The trial firing rate of a neuron was computed as total spikes over the full duration of trial divided by the trial duration. This resulted in inclusion of 380/563 and 360/529 for the before and during conditions, respectively. Restricting our analysis to neurons with an average trial firing rate greater than 5 spikes/s instead of 1 did not significantly change our results.

For each neuron, mean peri-stimulus time histogram (PSTH) was computed by binning spike times in 20ms non-overlapping bins (figure 1d, figure 6b). To compute the average population response in different tasks and epochs (figures 2–6), we normalized the mean PSTH of each neuron by its peak activity at the stimulus onset in the corresponding task and averaged the normalized PSTHs across all units, followed by a smoothing operation with a 3-point moving average.

Attention-related modulation: We used spike counts in the *Attend* and *Ignore* conditions during the delay period (1 – 1.5 s after stimulus onset, grey window in figure 2a, b) as signal and noise respectively to compute the area under the receiver operating characteristic curve (AUC). This AUC value determined a neuron's attention-related modulation. To evaluate the effect of SC inactivation on attention-related modulation we computed the distributions of AUC values before and during SC inactivation (figure 2c; see Results). We also computed the traditional attention-related modulation index (AMI) as $\frac{\mu_A - \mu_I}{\mu_A + \mu_I}$, where μ_A is the average spike count during the delay period (1 – 1.5 s after stimulus onset) in *Attend* condition and μ_I is the average spike count in *Ignore* condition. The effects reported in this manuscript do not depend on whether we use our attention-related modulation AUC measure or AMI (supplementary figure 1).

Fano factor index and neural correlations: In the same epoch as attention-related modulation (1 – 1.5 s after stimulus onset, grey window in figure 2a, b), we computed fano-factor index and neuronal correlation index for each neuron. Fano-factor index was computed as $\frac{f_A - f_I}{f_A + f_I}$, where f_A is the fano-factor during *Attend* and f_I, is the fano-factor during *Ignore*; f_A was computed as $\frac{\sigma_A}{\mu_A}$, where σ_A was the variance in spike count during *Attend* condition (supplementary figure 7). Neurons included in the fano-factor analysis were mean-matched following an approach described elsewhere (Churchland et al., 2010). Fano-factor results did not depend on whether we used the mean-matching approach or included all neurons in the analysis.

Neuronal correlation index was computed as the difference in inter-neuronal spike count correlations during *Attend* and *Ignore*. Spike count correlation between a pair of simultaneously recorded neurons was computed as a Pearson's correlation coefficient (MATLAB). Overall, we computed correlations for 4856 pairs of neurons before SC inactivation and 4341 pairs during SC inactivation (supplementary figure 7).

Change-related modulation: To compute an AUC value that determined a neuron's change-related modulation in activity we used spike counts in the *Attend* condition for change trials and time-matched no-change trials, during the post-change period (0.2 – 0.5 s epoch following the change, grey window in figure 3a, b).

Detect probability: The detect probability measure was computed for each neuron following established criteria (Cook and Maunsell, 2002). Briefly, detect probability is the AUC value obtained by comparing spike counts in the *Attend* condition for change trials, when the monkey successfully detected a stimulus change ("hit") to when the monkey failed to detect a stimulus change ("miss"), during the post-change period (0.2 – 0.5 s epoch following the change, grey window in figure 4a, b).

Object selectivity: To compute an AUC value for each neuron's object selectivity in the object-tuning task, we used spike counts for the object image compared to the corresponding

scrambled version of the image during the 0.08 – 0.12 s epoch after the image onset (grey window in figure 6d, e).

We evaluated the effect of SC inactivation on attention-related modulation (figure 2c, 5e), change-related modulation (figure 3c, 5h), detect probability (figure 4c, 5k) and object selectivity (figure 6f) by comparing the distributions of AUC values before and during SC inactivation (see Results).

Continuous isolation of neurons in "before" and "during" datasets—To identify the neurons that were likely to have been continuously isolated throughout the "before" and "during" phases of the same session, we used a previously described and validated method used on similar datasets to this study (Herman et al., 2020). It was built on established methods for identifying individual neurons recorded across successive days on the same channel of multi-channel "utah" arrays (Eleryan et al., 2014; Fraser and Schwartz, 2012). Overall, we identified a "continuously isolated" subpopulation of 255/380 fSTS neurons that were most likely to have been recorded throughout the "before" and "during" phases of each session (114 from monkey #1 and 141 from monkey #2).

Briefly, the continuous isolation approach involved two steps. In step 1, we concatenated the 'before" and "during" electrophysiological recordings and resorted the continuous voltage trace using an advanced spike sorting algorithm (kilosort2) that is particularly suitable for tracking single neurons drifting across recording contacts over the course of a session. In step 2, we established stable isolation criteria by splitting data collected in the "before" phase into two halves and comparing spike metrics from one half to the other. We then applied these stable isolation criteria on spike metrics for each neuron in "before" and "during" phases and considered those neurons that met our stable isolation criteria as "continuously isolated neurons". It is important to note that stable isolation criterion relies on the assumption that neurons were stable and clearly isolated for the total duration of the "before" phase. Given that each recording session started with an hour-long waiting period in which the tissue was allowed to relax around the electrode, this assumption is likely met.

To establish stable isolation criteria, we used data collected in the "before" phase to identify "true positive" (same neuron) and "true negative" (different neuron) example cases. All 438 clearly isolatable waveforms were considered true positives: we built true positive distributions of several waveform metrics (detailed below) by comparing individual metrics for each waveform computed on data from the 1st half of "before" phase to the same metric computed on data from the 2nd half of "before" phase. Similarly, we built true-negative distributions by identifying 187 instances in which two different waveforms appeared on the same electrode contact, and comparing spike metrics computed on data for one waveform from the 1st half of "before" phase to metrics computed on data for the other waveform from the 2nd half of "before" phase. The five waveform metrics we considered were: (1) average waveform "shape", (2) waveform amplitude (peak-to-trough), (3) waveform power, (4) time from peak-to-trough, and (5) inter-spike-interval (ISI) distribution. For "shape" metric, we compared two average waveform "shapes" by computing their Pearson correlation (each average waveform comprised 2 ms of data sampled at 40kHz or 81 samples). For all other four metrics, we computed the Bhattacharya distance between distributions of metric values

(for example, between distributions of time from peak-to-trough values). These steps resulted in 5 spike-metric values for each true positive and true negative which we then used to construct a 5-fold cross-validated regularized logistic regression model (the “continuous isolation model”; regularization was used to contend with correlations amongst spike-metric predictors). We then applied the continuous isolation model to comparisons of spike metrics in “before” phase to those metrics in “during” phase in all neurons recorded throughout before and during phases of each experiment. Finally, we labelled those neurons with a model value greater than 0.95 as “continuously isolated neurons” (67%; 255/380). Importantly, this method was validated on single-unit recordings, in which units were tracked by a human experimenter throughout the session (Herman et al., 2020).

Supplementary Material

Refer to Web version on PubMed Central for supplementary material.

Acknowledgments:

We thank Tom Ruffner and Nick Nichols for technical support. We are grateful to Fabrice Arcizet, James Herman, and Lupeng Wang for helpful discussions and input. We thank James Herman for providing code to determine continuously isolated neurons. This work was supported by the National Eye Institute Intramural Research Program (ZIA EY000511) and National Institute of Mental Health Intramural Research Program (ZIA MH002838) at the National Institutes of Health.

References

Basso MA, and May PJ (2017). Circuits for Action and Cognition: A View from the Superior Colliculus. Annu. Rev. Vis. Sci. 3, 197–226. [PubMed: 28617660]

Beltramo R, and Scanziani M (2019). A collicular visual cortex: Neocortical space for an ancient midbrain visual structure. Science 363, 64–69. [PubMed: 30606842]

Bennett C, Gale SD, Garrett ME, Newton ML, Callaway EM, Murphy GJ, and Olsen SR (2019). Higher-Order Thalamic Circuits Channel Parallel Streams of Visual Information in Mice. Neuron 102, 477–492.e5. [PubMed: 30850257]

Bogadhi AR, Bollimunta A, Leopold DA, and Krauzlis RJ (2018). Brain regions modulated during covert visual attention in the macaque. Sci. Rep. 8, 15237. [PubMed: 30323289]

Bogadhi AR, Bollimunta A, Leopold DA, and Krauzlis RJ (2019). Spatial attention deficits are causally linked to an area in macaque temporal cortex. Curr. Biol. 29, 726–736.e4. [PubMed: 30773369]

Bondy AG, Haefner RM, and Cumming BG (2018). Feedback determines the structure of correlated variability in primary visual cortex. Nat. Neurosci. 21, 598–606. [PubMed: 29483663]

Boussaoud D, Desimone R, and Ungerleider LG (1992). Subcortical connections of visual areas MST and FST in macaques. Vis Neurosci 9, 291–302. [PubMed: 1390388]

Brainard DH (1997). The Psychophysics Toolbox. Spat Vis 10, 433–436. [PubMed: 9176952]

Bruce C, Desimone R, and Gross CG (1981). Visual properties of neurons in a polysensory area in superior temporal sulcus of the macaque. J. Neurophysiol. 46, 369–384. [PubMed: 6267219]

Caspari N, Janssens T, Mantini D, Vandenberghe R, and Vanduffel W (2015). Covert shifts of spatial attention in the macaque monkey. J. Neurosci. 35, 7695–7714. [PubMed: 25995460]

Cavanaugh J, and Wurtz RH (2004). Subcortical modulation of attention counters change blindness. J. Neurosci. 24, 11236–11243. [PubMed: 15601929]

Chen LL, Goffart L, and Sparks DL (2001). A simple method for constructing microinjectrodes for reversible inactivation in behaving monkeys. J. Neurosci. Methods 107, 81–85. [PubMed: 11389944]

Churchland MM, Yu BM, Cunningham JP, Sugrue LP, Cohen MR, Corrado GS, Newsome WT, Clark AM, Hosseini P, Scott BB, et al. (2010). Stimulus onset quenches neural variability: a widespread cortical phenomenon. Nat. Neurosci. 13, 369–378. [PubMed: 20173745]

Cohen MR, and Newsome WT (2009). Estimates of the contribution of single neurons to perception depend on timescale and noise correlation. J. Neurosci. 29, 6635–6648. [PubMed: 19458234]

Cook EP, and Maunsell JHR (2002). Dynamics of neuronal responses in macaque MT and VIP during motion detection. Nat. Neurosci. 5, 985–994. [PubMed: 12244324]

Desimone R, and Ungerleider LG (1986). Multiple visual areas in the caudal superior temporal sulcus of the macaque. J. Comp. Neurol. 248, 164–189. [PubMed: 3722457]

Dominguez-Vargas A-U, Schneider L, Wilke M, and Kagan I (2017). Electrical Microstimulation of the Pulvinar Biases Saccade Choices and Reaction Times in a Time-Dependent Manner. J. Neurosci. 37, 2234–2257. [PubMed: 28119401]

Eastman KM, and Huk AC (2012). PLDAPS: A hardware architecture and software toolbox for neurophysiology requiring complex visual stimuli and online behavioral control. Front Neuroinformatics 6, 1.

Eleryan A, Vaidya M, Southerland J, Badreldin IS, Balasubramanian K, Fagg AH, Hatsopoulos N, and Oweiss K (2014). Tracking single units in chronic, large scale, neural recordings for brain machine interface applications. Front Neuroengineering 7, 23.

Felleman DJ, and Van Essen DC (1991). Distributed hierarchical processing in the primate cerebral cortex. Cereb. Cortex 1, 1–47. [PubMed: 1822724]

Fraser GW, and Schwartz AB (2012). Recording from the same neurons chronically in motor cortex. J. Neurophysiol. 107, 1970–1978. [PubMed: 22190623]

Gold JI, and Shadlen MN (2007). The neural basis of decision making. Annu. Rev. Neurosci. 30, 535–574. [PubMed: 17600525]

Harting JK, Huerta MF, Frankfurter AJ, Strominger NL, and Royce GJ (1980). Ascending pathways from the monkey superior colliculus: an autoradiographic analysis. J. Comp. Neurol. 192, 853–882. [PubMed: 7419758]

Herman JP, Arcizet F, and Krauzlis RJ (2020). Attention-related modulation of caudate neurons depends on superior colliculus activity. Elife 9.

Hilgetag CC, O'Neill MA, and Young MP (2000). Hierarchical organization of macaque and cat cortical sensory systems explored with a novel network processor. Philos. Trans. R. Soc. Lond. B, Biol. Sci. 355, 71–89. [PubMed: 10703045]

Hung CP, Kreiman G, Poggio T, and DiCarlo JJ (2005). Fast readout of object identity from macaque inferior temporal cortex. Science 310, 863–866. [PubMed: 16272124]

Jellema T, and Perrett DI (2003). Cells in monkey STS responsive to articulated body motions and consequent static posture: a case of implied motion? Neuropsychologia 41, 1728–1737. [PubMed: 14527537]

Kilintari M, Raos V, and Savaki HE (2014). Involvement of the superior temporal cortex in action execution and action observation. J. Neurosci. 34, 8999–9011. [PubMed: 24990920]

Krauzlis RJ, Lovejoy LP, and Zénon A (2013). Superior colliculus and visual spatial attention. Annu. Rev. Neurosci. 36, 165–182. [PubMed: 23682659]

Krauzlis RJ, Bogadhi AR, Herman JP, and Bollimunta A (2018). Selective attention without a neocortex. Cortex 102, 161–175. [PubMed: 28958417]

Kreiman G, Hung CP, Kraskov A, Quiroga RQ, Poggio T, and DiCarlo JJ (2006). Object selectivity of local field potentials and spikes in the macaque inferior temporal cortex. Neuron 49, 433–445. [PubMed: 16446146]

Lovejoy LP, and Krauzlis RJ (2010). Inactivation of primate superior colliculus impairs covert selection of signals for perceptual judgments. Nat. Neurosci. 13, 261–266. [PubMed: 20023651]

Mitchell JF, Sundberg KA, and Reynolds JH (2009). Spatial attention decorrelates intrinsic activity fluctuations in macaque area V4. Neuron 63, 879–888. [PubMed: 19778515]

Mysore SG, Vogels R, Raiguel SE, Todd JT, and Orban GA (2010). The selectivity of neurons in the macaque fundus of the superior temporal area for three-dimensional structure from motion. J. Neurosci. 30, 15491–15508. [PubMed: 21084605]

Pachitariu M, Steinmetz NA, Kadir SN, Carandini M, and Harris KD (2016). Fast and accurate spike sorting of high-channel count probes with KiloSort. Adv. Neural Inf. Process. Syst. 4448.

Patel GH, Yang D, Jamerson EC, Snyder LH, Corbetta M, and Ferrera VP (2015). Functional evolution of new and expanded attention networks in humans. Proc. Natl. Acad. Sci. USA 112, 9454–9459. [PubMed: 26170314]

Rolls ET (2000). Functions of the primate temporal lobe cortical visual areas in invariant visual object and face recognition. Neuron 27, 205–218. [PubMed: 10985342]

Rosenberg A, Wallisch P, and Bradley DC (2008). Responses to direction and transparent motion stimuli in area FST of the macaque. Vis Neurosci 25, 187–195. [PubMed: 18442441]

Squire RF, Noudoost B, Schafer RJ, and Moore T (2013). Prefrontal contributions to visual selective attention. Annu. Rev. Neurosci. 36, 451–466. [PubMed: 23841841]

Sridharan D, Steinmetz NA, Moore T, and Knudsen EI (2017). Does the Superior Colliculus Control Perceptual Sensitivity or Choice Bias during Attention? Evidence from a Multialternative Decision Framework. J. Neurosci. 37, 480–511. [PubMed: 28100734]

Stemmann H, and Freiwald WA (2019). Evidence for an attentional priority map in inferotemporal cortex. Proc. Natl. Acad. Sci. USA 116, 23797–23805. [PubMed: 31685625]

Tohmi M, Meguro R, Tsukano H, Hishida R, and Shibuki K (2014). The extrageniculate visual pathway generates distinct response properties in the higher visual areas of mice. Curr. Biol. 24, 587–597. [PubMed: 24583013]

Tsao DY, Freiwald WA, Knutsen TA, Mandeville JB, and Tootell RBH (2003). Faces and objects in macaque cerebral cortex. Nat. Neurosci. 6, 989–995. [PubMed: 12925854]

Tsao DY, Freiwald WA, Tootell RBH, and Livingstone MS (2006). A cortical region consisting entirely of face-selective cells. Science 311, 670–674. [PubMed: 16456083]

Ward MK, Bolding MS, Schultz KP, and Gamlin PD (2015). Mapping the macaque superior temporal sulcus: functional delineation of vergence and version eye-movement-related activity. J. Neurosci. 35, 7428–7442. [PubMed: 25972171]

Willenbockel V, Sadr J, Fiset D, Horne GO, Gosselin F, and Tanaka JW (2010). Controlling low-level image properties: the SHINE toolbox. Behav. Res. Methods 42, 671–684. [PubMed: 20805589]

Zénon A, and Krauzlis RJ (2012). Attention deficits without cortical neuronal deficits. Nature 489, 434–437. [PubMed: 22972195]

Highlights

- fSTS neurons exhibit attention modulation, event detection and object selectivity
- These high-level visual properties are all dependent on activity from the SC
- Dependence on SC activity is observed for both motion and stationary stimuli
- SC activity may prioritize cortical processing of task-relevant events and objects

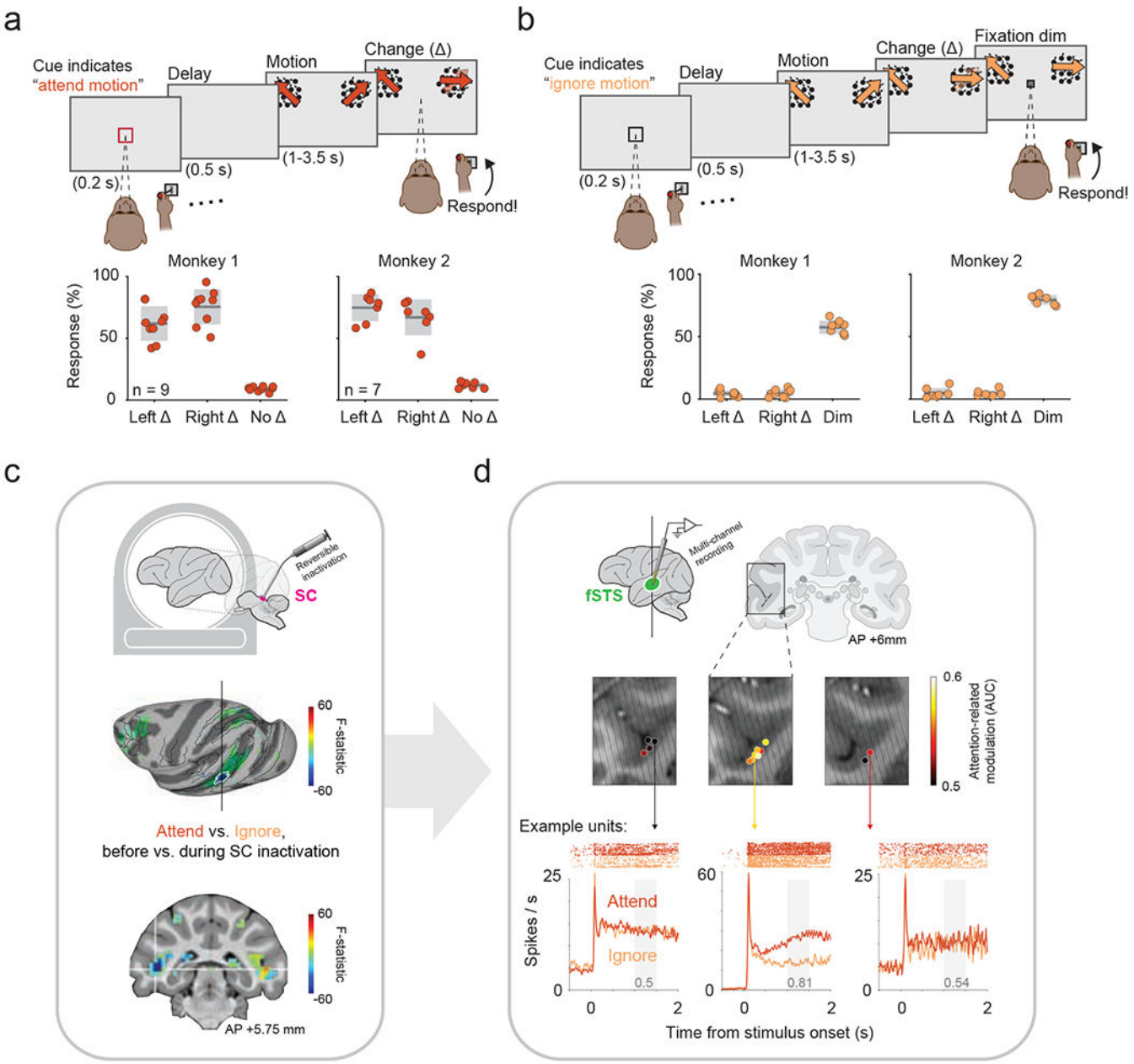

Figure 1. Identification of the fSTS region as dependent on SC activity

a. Top: Red cue instructed monkey to attend motion stimuli and report changes in motion direction (Δ). Bottom: response rates for left and right Δ (hits) and "no-Δ" (catch) trials. Individual sessions are plotted over gray box indicating mean ± sd.

b. Top: Black cue instructed monkey to ignore motion-changes and report a dim in fixation spot. Bottom: response rates for left and right Δ (false alarms) and for dim (hits). Same format as a.

c. Functional activations with and without SC inactivation identified a circumscribed region (blue colored patch outlined in white) in fSTS whose modulation was the most dependent on SC activity.

d. Coronal slices of the fSTS are overlaid with average attention-related modulation (measured as AUC, see Methods) across neurons recorded in each location (colored spots). Oblique lines indicate electrode approach. Bottom: Example neuronal responses to *Attend* and *Ignore* conditions and their corresponding modulation values (gray text), from three recording locations exhibiting poor (left example), good (center), and intermediate (right) attention-related modulations.

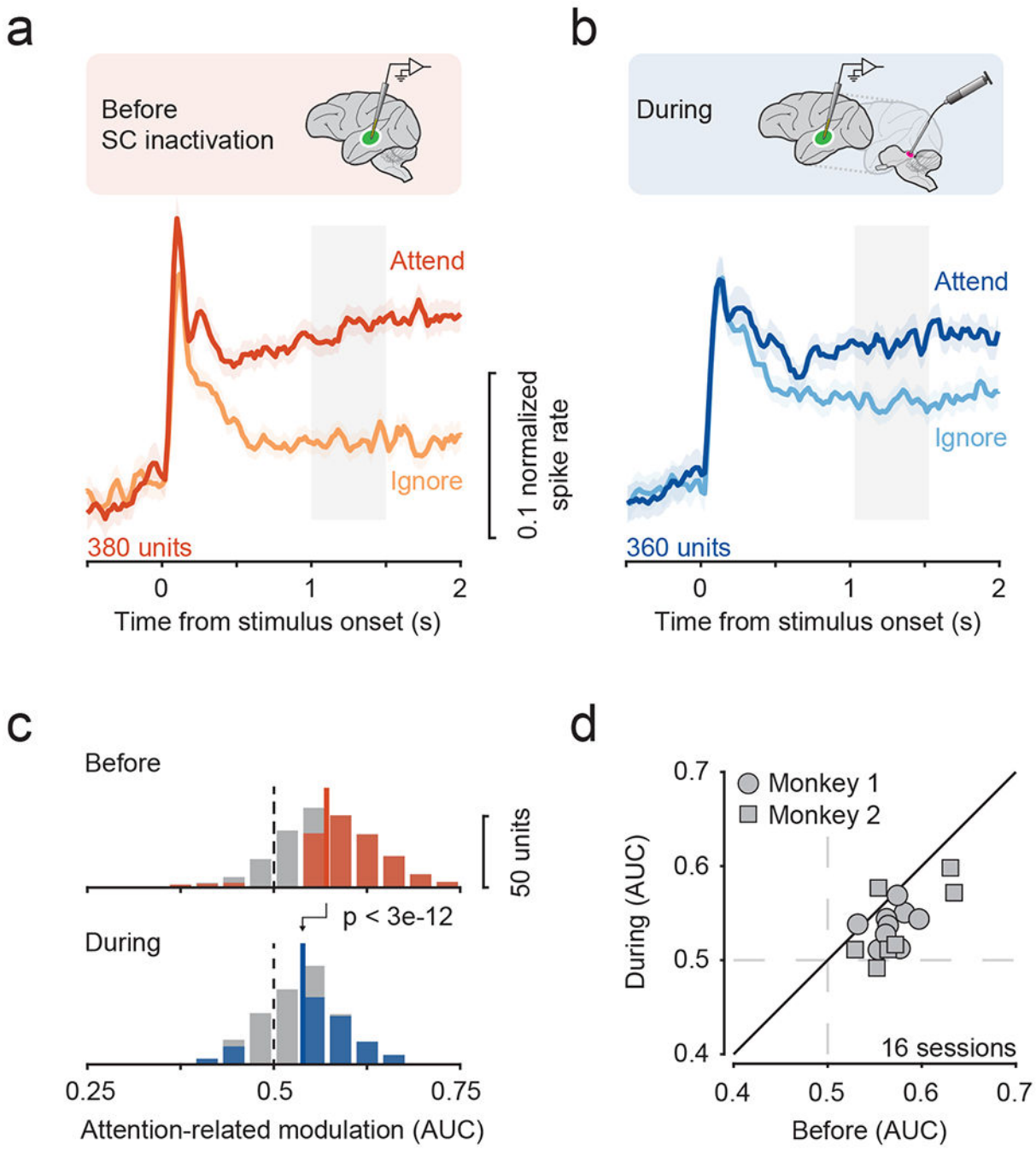

Figure 2. Attention-related modulation in fSTS depends on SC activity

a, b. Population average of the normalized responses to motion stimulus in *Attend* and *Ignore* conditions before (a) and during (b) SC inactivation. Error bars indicate 68.2% CI. Grey window indicates time period used for computing attention-related modulation.

c. Distribution of attention-related modulation values across neurons before (median = 0.57) and during SC inactivation (median = 0.54). Solid and dotted lines indicate median and no modulation, respectively. Colored shading indicates significance for individual neurons ($p < 0.05$, bootstrap test).

d. Average attention-related modulation across simultaneously recorded neurons within a session (mean ± sd = 23.75 ± 8.72), before and during SC inactivation.
See also figures S1–S5.

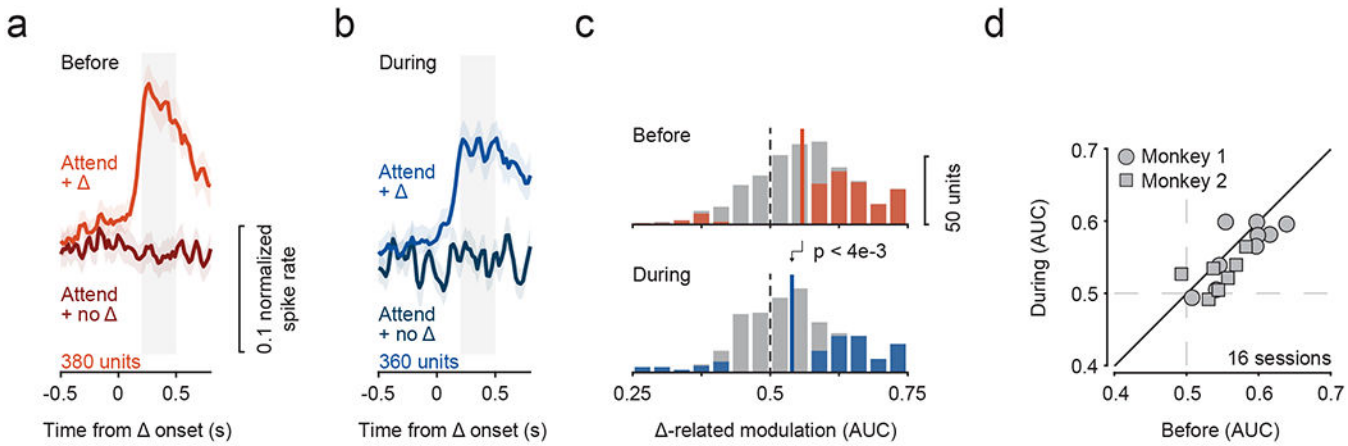

Figure 3. Change-evoked activity in fSTS neurons depends on SC activity

a, b. Population average of the normalized responses to motion-change (Δ) and no-change (no Δ) events in the *Attend* condition before (a) and during (b) SC inactivation. No Δ trials were aligned to time-matched Δ trials. Grey window indicates time period used for computing change-related modulation. Error bars: 68.2% CI.

c. Distribution of change-related modulation values before (median = 0.56) and during SC inactivation (median = 0.54). Solid and dotted lines indicate median and no modulation, respectively. Colored shading indicates significance for individual neurons ($p < 0.05$, bootstrap test).

d. Effect of SC inactivation on change-related modulation across sessions.

See also figure S3.

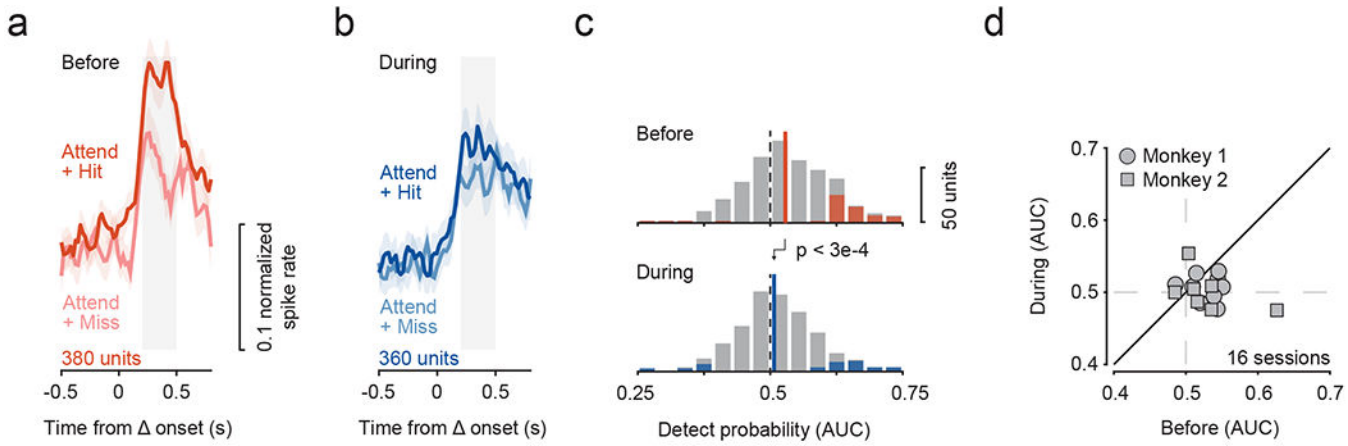

Figure 4. Detect probability in fSTS neurons depends on SC activity

a, b. Population average of the normalized responses to successfully detected motion-change (Δ) trials ("hit") and undetected trials ("miss") in the *Attend* condition before (a) and during (b) SC inactivation. Grey window indicates time period used for computing detection-related modulation (i.e. detect probability, see Methods). Error bars: 68.2% CI.

c. Distribution of detect probability values before (median = 0.53) and during SC inactivation (median = 0.51). Solid and dotted lines indicate median and no modulation, respectively. Colored shading indicates significance for individual neurons ($p < 0.05$, bootstrap test).

d. Effect of SC inactivation on detect probability across sessions.

See also figure S3.

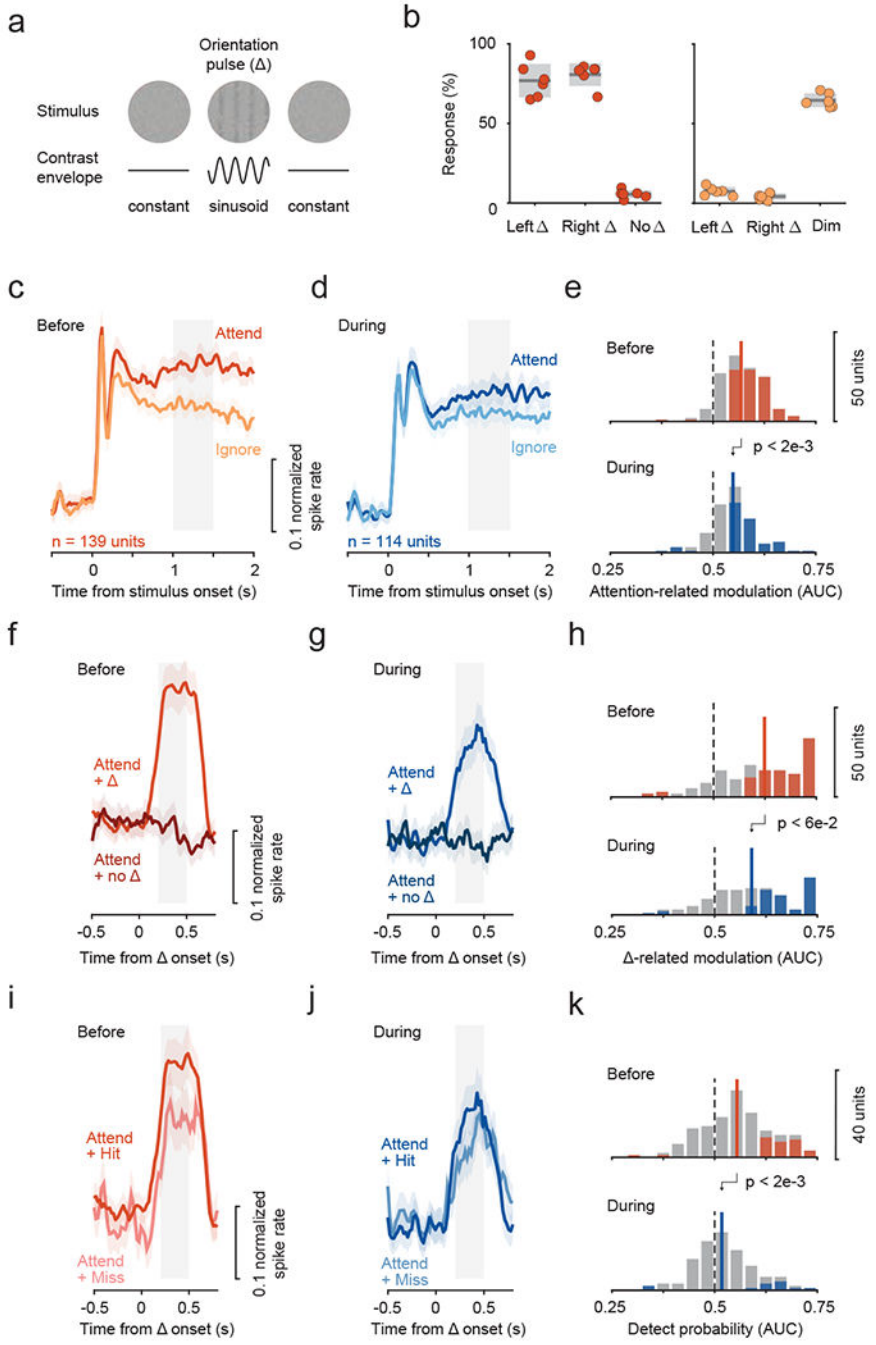

Figure 5. Effect of SC inactivation on attention-related modulation, change-evoked activity and detect probability in fSTS neurons was not specific to motion stimuli

a. The monkeys' task was to detect the brief appearance (0.5 s) of a 2nd order orientation pulse stimulus, that cannot be detected from its motion energy, from a dynamic white noise stimulus. The pulse was constructed by applying a sinusoidal contrast envelope on the white noise stimulus (see Methods).

b. Behavioral performance in the task for the attend (left panel) and ignore (right panel) conditions (similar format to figure 1a, b).

c-e. Attention-related modulation before and during SC inactivation (same format as figure 2a–c).

f-h. Change-related activity before and during SC inactivation (same format as figure 3a–c).

i-k. Detect probability before and during SC inactivation (same format as figure 4a–c).

See also figure S2.

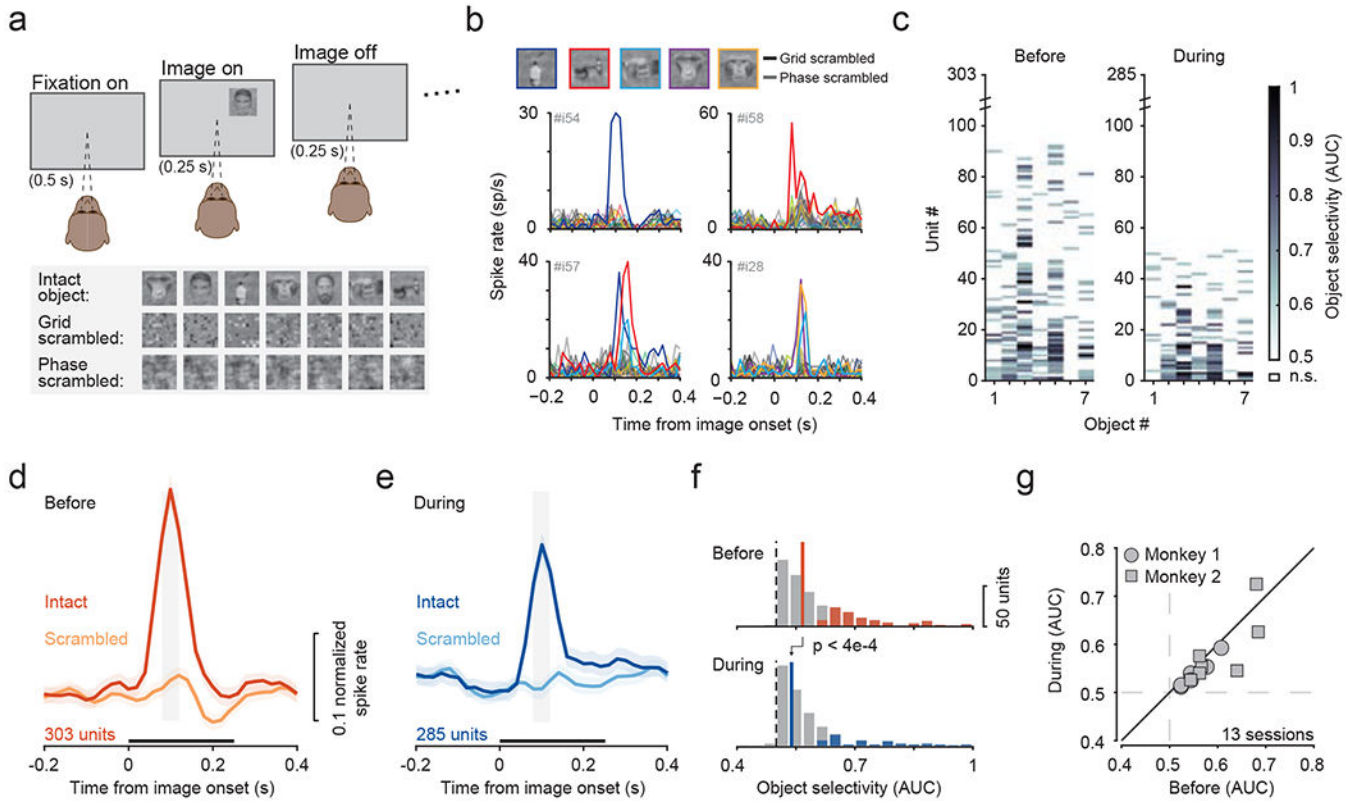

Figure 6. Object selectivity in fSTS neurons depends on SC activity

a. Monkeys fixated a central spot while either object, grid-scrambled, or phase-scrambled images were presented.

b. Example neurons that responded selectively to individual object images.

c. Object selectivity values for individual neurons, sorted by number of objects selective for, before and during SC inactivation. Non-significant (n.s.) selectivity ($p > 0.05$, bootstrap test) is shown as white.

d, e. Population average of normalized responses to the most selective object and the corresponding scrambled object, before (d) and during (e) SC inactivation. Grey window indicates time period used for computing object selectivity. Black bar above abscissa indicates the duration of image presentation. Error bars: 68.2% CI.

f. Distribution of object selectivity values before (median = 0.57) and during SC inactivation (median = 0.55). Solid and dotted lines indicate median and no selectivity, respectively. Colored shading indicates significance for individual neurons ($p < 0.05$, bootstrap test).

g. Effect of SC inactivation on object-selectivity across sessions.

See also figure S6.

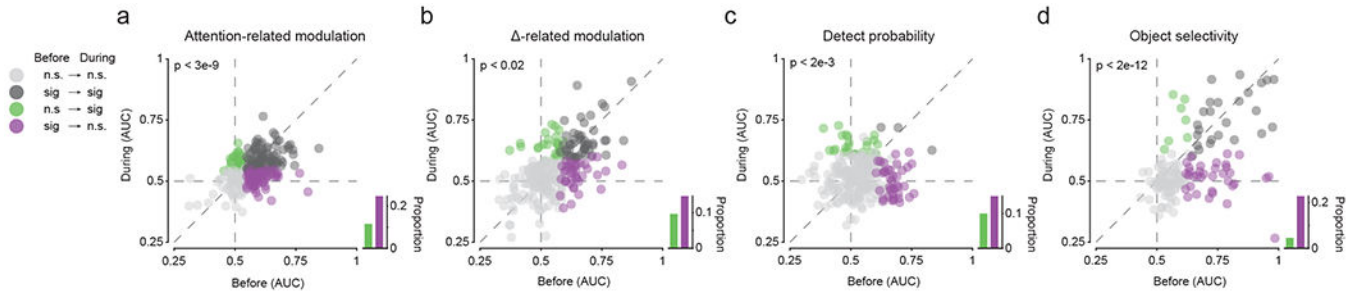

Figure 7. Effects of SC inactivation on continuously isolated fSTS neurons

a. A paired comparison of attention-related modulation (AUC) before and during SC inactivation in single continuously isolated fSTS neurons (filled circles). Different colors represent statistically significant modulation in 'before' vs 'during' (see legend; $p < 0.05$, bootstrap test). The bar plot (inset) compares the proportion of neurons with significant modulation in 'before' but not 'during' (purple) to those with significant modulation in 'during' but not 'before' (green).

b-d. Same format as in **a** for change-related (Δ-related) modulation (**b**), detect probability (**c**) and object selectivity (**d**).

KEY RESOURCES TABLE

REAGENT or RESOURCE	**SOURCE**	**IDENTIFIER**
Experimental Models: Organisms/Strains		
Macaca Mulatta	NEI Primate Facility	N/A
Software and Algorithms		
MATLAB	Mathworks	RRID: SCR_001622
OmniPlex	Plexon, Inc	RRID:SCR_014803
KiloSort	Cortex Lab	RRID:SCR_016422
Other		
VIEWPixx	VPixx Technologies	Cat# VPX-VPX-2001C; RRID:SCR_013271
Eyelink	SR Research	Cat# 1000; RRID:SCR_009602
Plexon V-probe	Plexon, Inc	RRID:SCR_018784